Star formation in Galaxies

(good refs: Kennicutt 1998 ARAA; Kennicutt & Evans 2012)

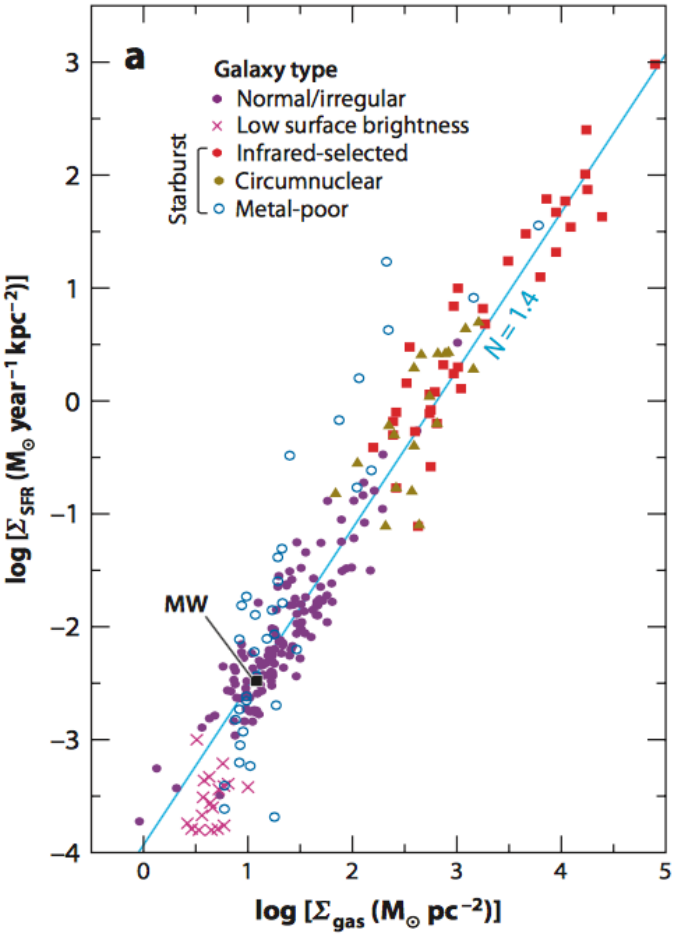

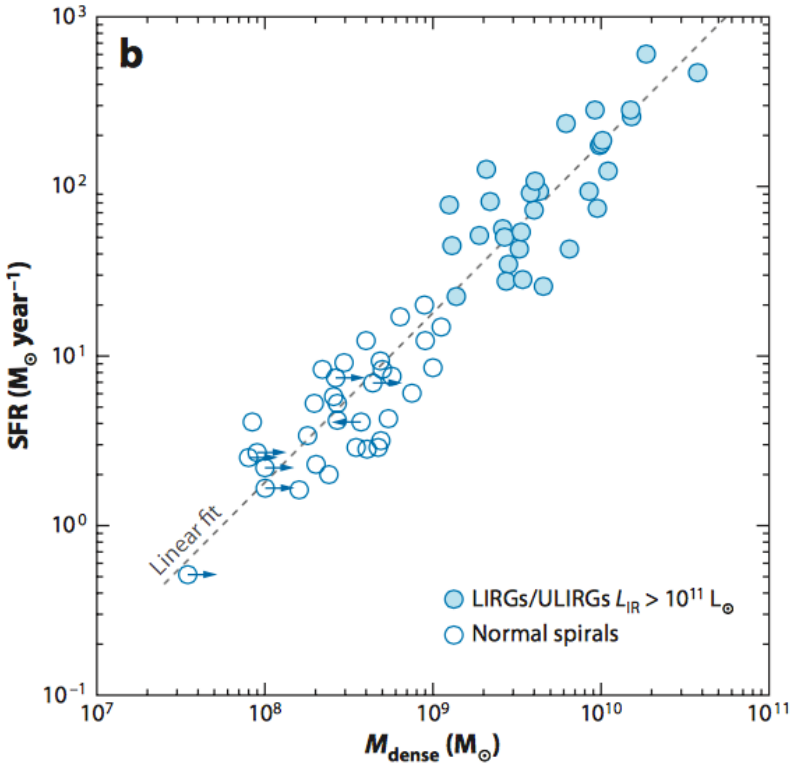

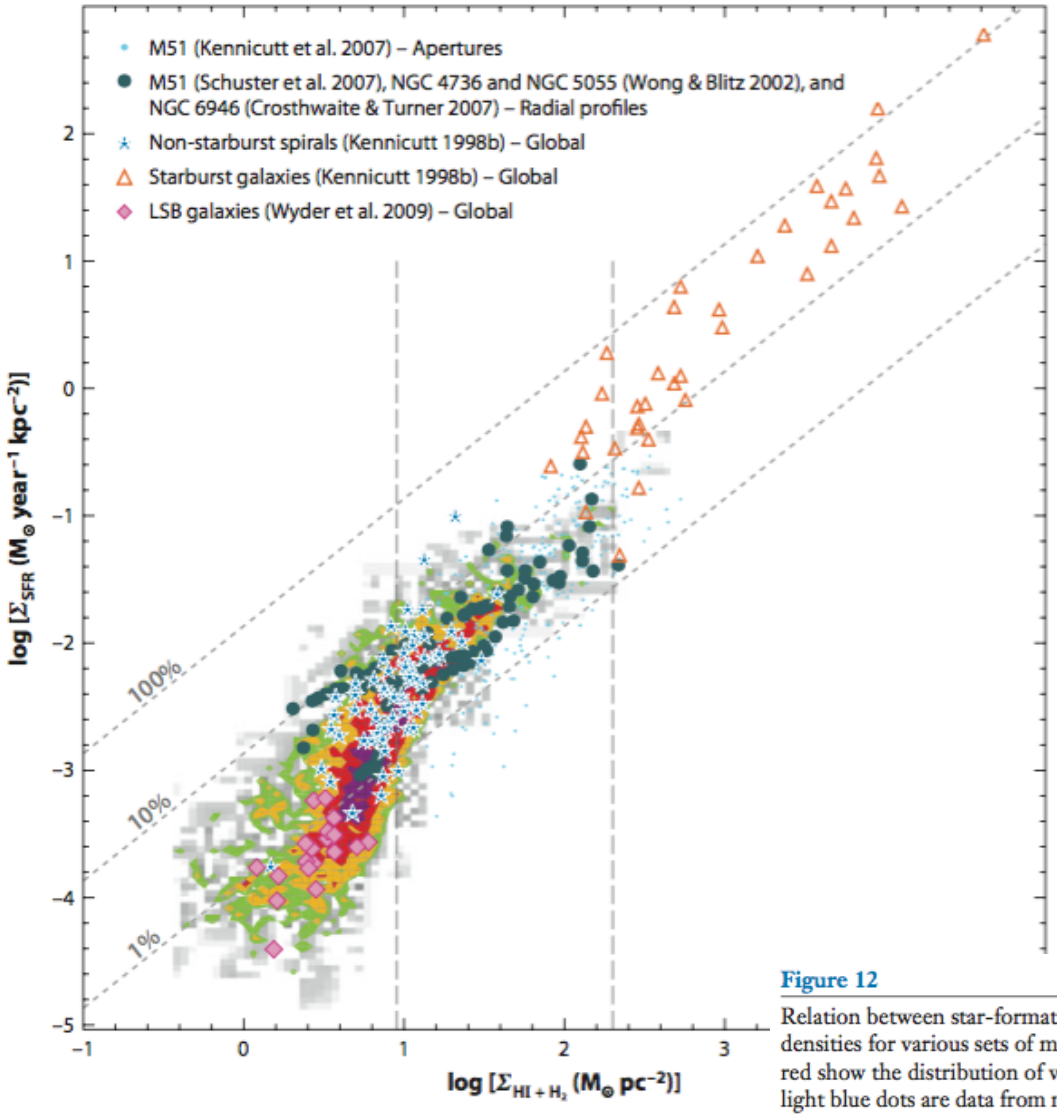

Figure 12

Relation between star-formation-rate (SFR) surface densities and total (atomic and molecular) gas surface densities for various sets of measurements (from Bigiel et al. 2008). Regions colored gray, green, yellow, and red show the distribution of values from measurements of subregions of SINGS galaxies. Overplotted as light blue dots are data from measurements in individual apertures in M51 (Kennicutt et al. 2007). Data from radial profiles from M51 (Schuster et al. 2007), NGC 4736 and NGC 5055 (Wong & Blitz 2002), and NGC 6946 (Crosthwaite & Turner 2007) are shown as dark blue filled circles. The disk-averaged measurements from 61 normal spiral galaxies (*dark blue stars*) and 36 starburst galaxies (*orange triangles*) from Kennicutt (1998b) are also shown. The magenta-filled diamonds show global measurements from 20 low-surface-brightness (LSB) galaxies (Wyder et al. 2009). In all cases, calibrations of initial mass function (IMF), X(CO), etc., were placed on a common scale. The three dotted gray diagonal lines extending from lower left to upper right reflect a constant global star-formation efficiency. The two vertical lines denote regimes that correspond roughly to those discussed in Section 6 of this review. Figure taken from Bigiel et al. (2008). Reproduced by permission of the AAS.

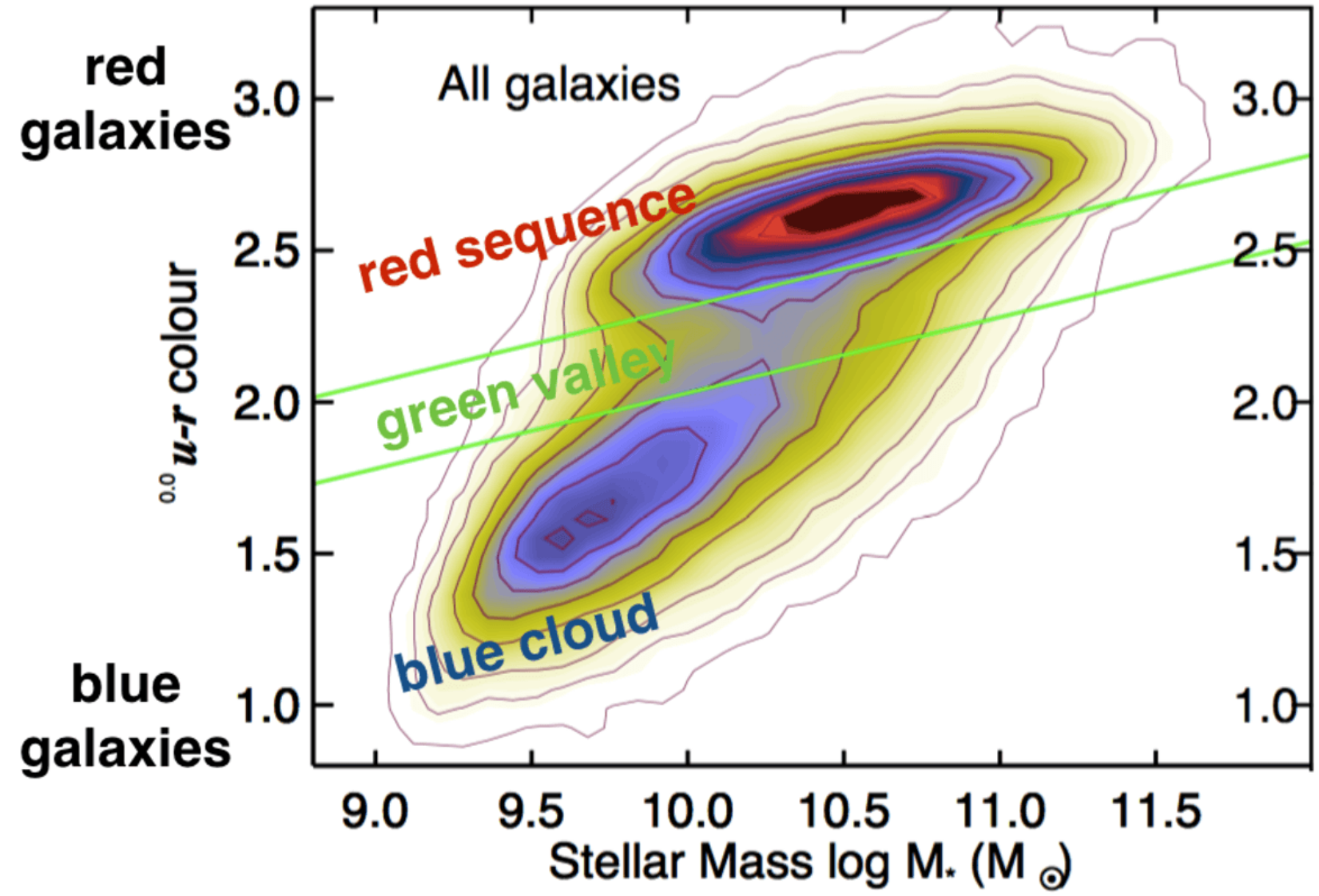
red galaxies
blue galaxies
All galaxies
red sequence
green valley
blue cloud
$^{0.0}u$-r colour
3.0
2.5
2.0
1.5
1.0
9.0
9.5
10.0
10.5
11.0
11.5
Stellar Mass log M* (M⊙)

Quenching™: How to Move from the Blue Cloud™ Through the Green Valley™ and to the Red Sequence™ in 9 Easy Steps in the Face of Downsizing™

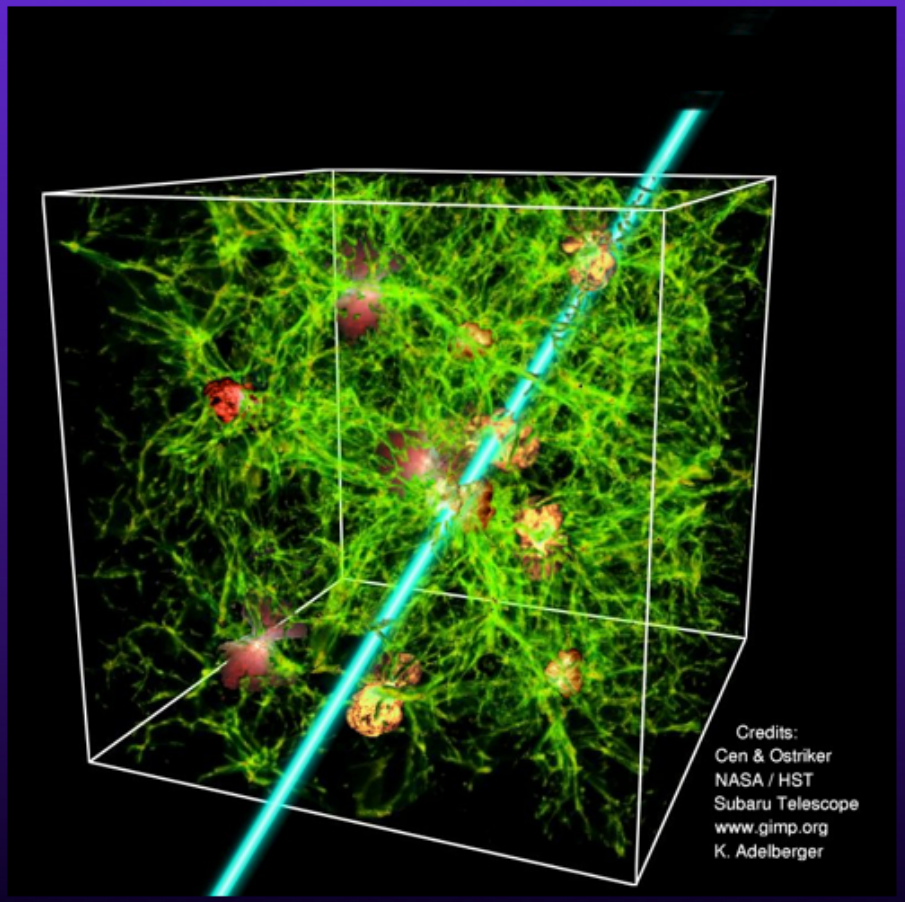

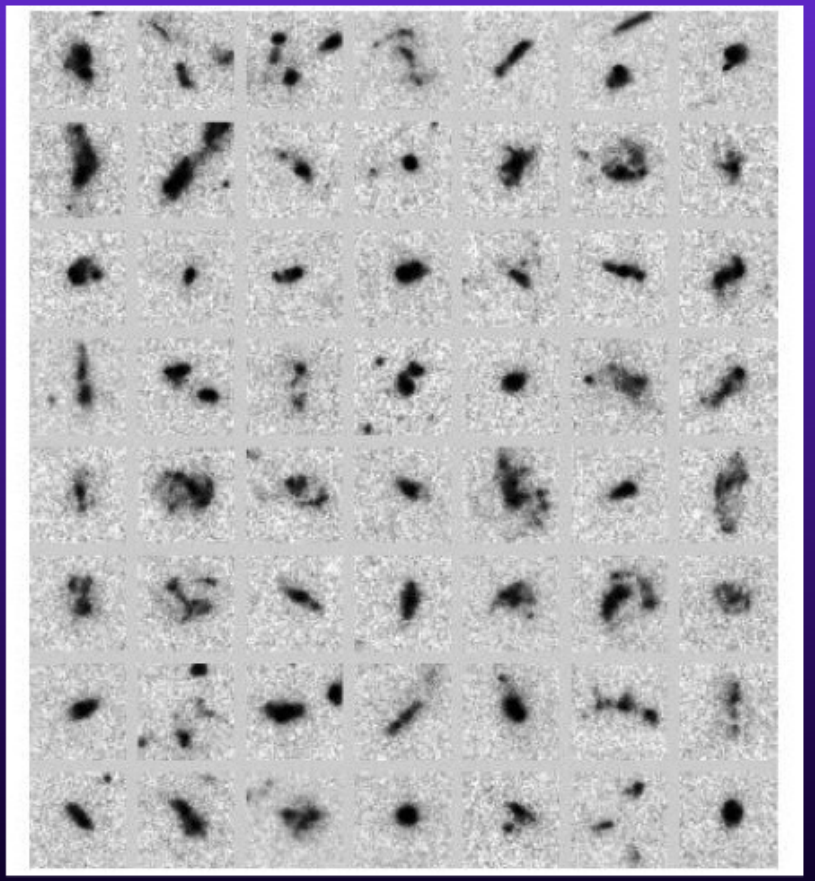

“Star-forming Main Sequence”?

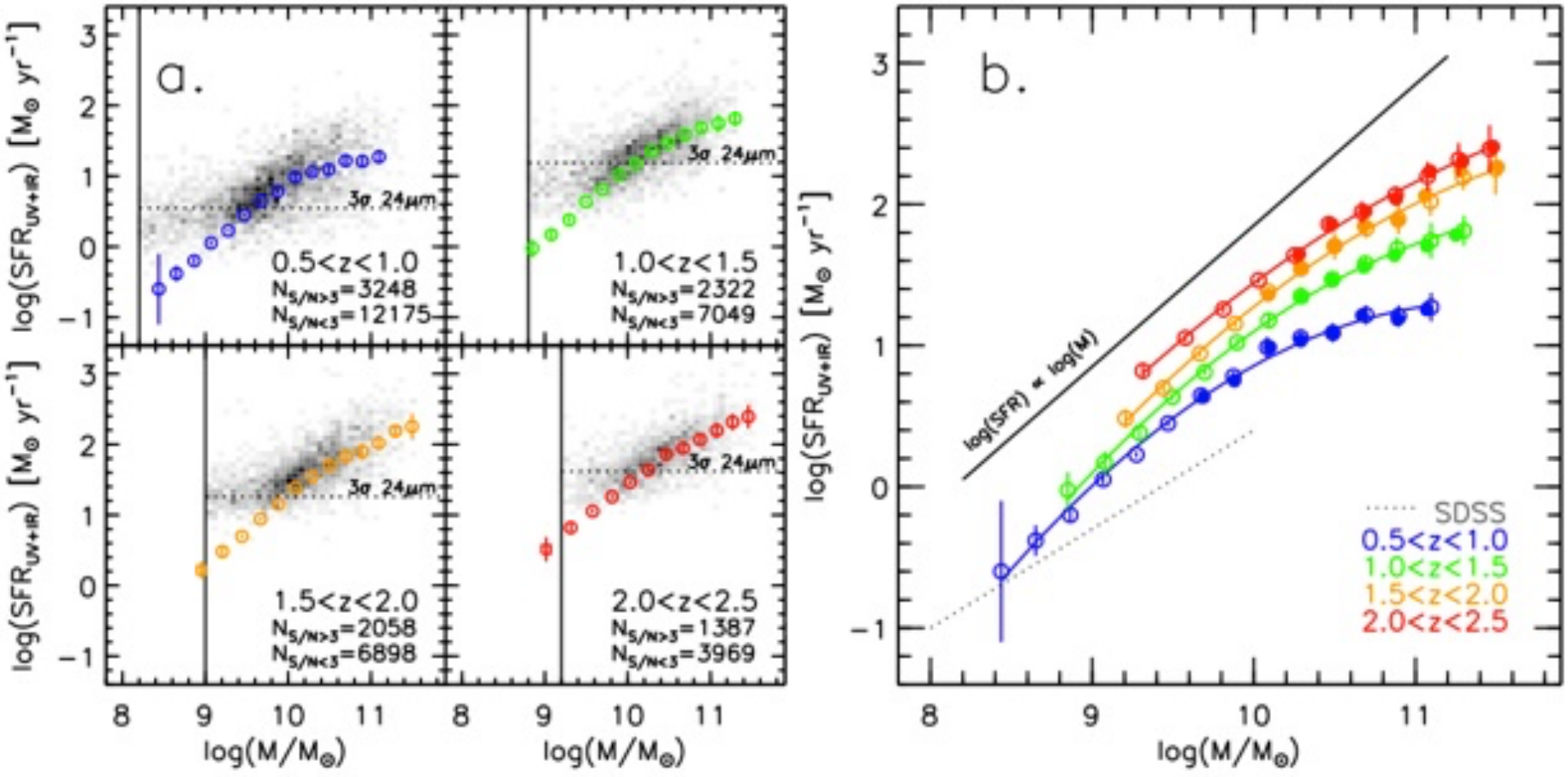

Credit: K. Whittaker

Kennicutt 1992, ApJS 79, 255

1992ApJS...79..255K

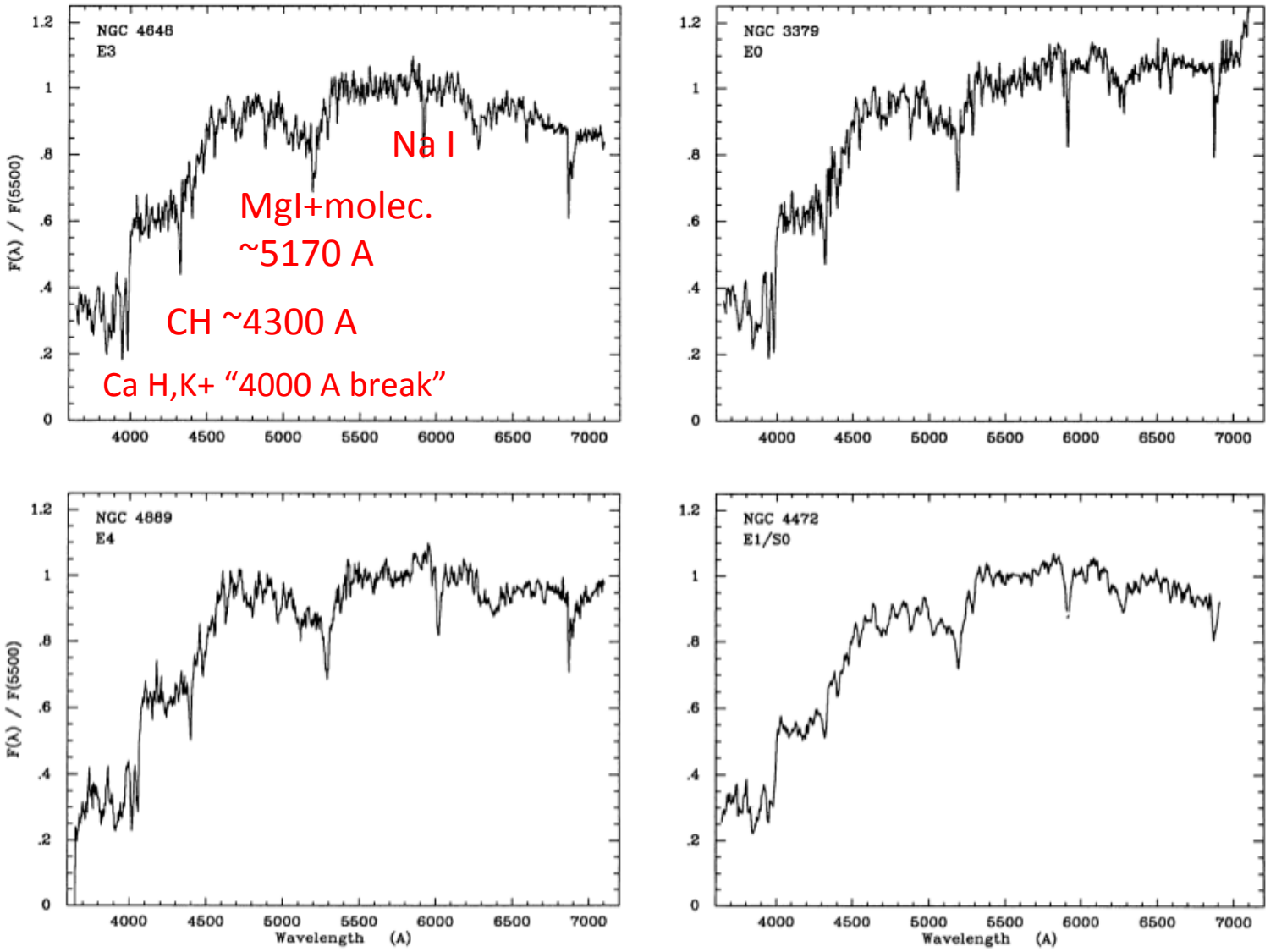

FIG. 5.—Integrated spectra of four elliptical galaxies. The spectrum of NGC 4472 (*lower right*) was obtained at lower resolution with the IRS scanner.

Kennicutt 1992, ApJS 79, 255

1992ApJS...79..255K

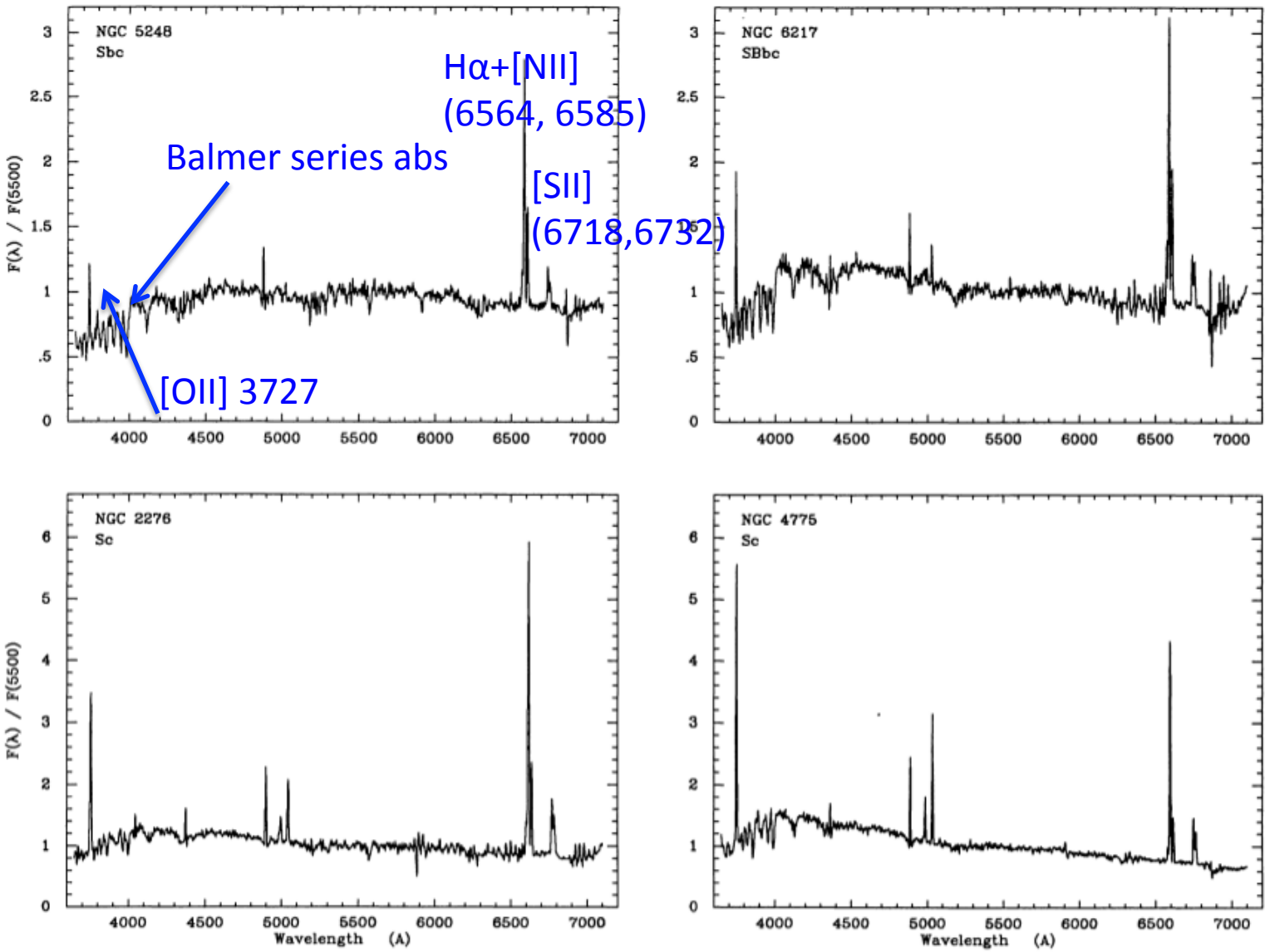

FIG. 9.—Integrated spectra of four Sbc–Sc galaxies, selected to illustrate the range in emission-line strengths and blue continuum properties. See Fig. 10 for other examples.

Kennicutt 1992, ApJS 79, 255

1992ApJS...79..255K

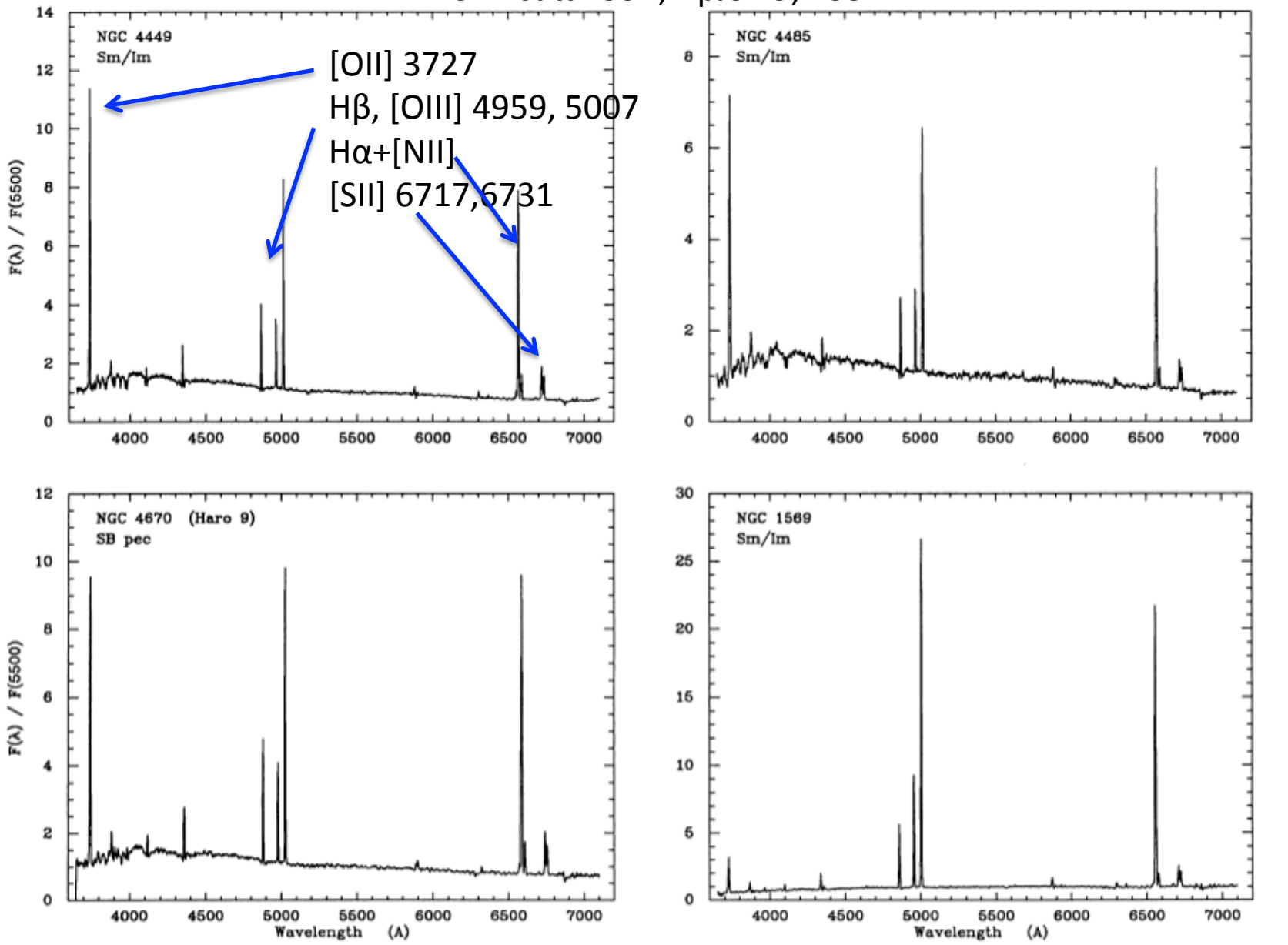

FIG. 11.—Integrated spectra of three Magellanic irregular galaxies (NGC 4449, 4485, 1569), and one peculiar galaxy with a very similar spectrum (NGC 4670).

Prominent Nebular Emission Lines (rest-frame optical)

[OII] 3727,3729 Ratio sensitive to electron density, strong at high metallicity

[OIII] 4959,5007 Ratio fixed (1:3) but [OIII]/Hβ sensitive to ionizing source; strongest line for $Z < 0.6Z_{\odot}$

Hα/Hβ (6564/4861) First counts ionizing photons, ratio should be ~2.9 in the absence of reddening/extinction

[NII] (6549, 6585) Ratio of two lines fixed (1:3) but [NII]/Hα sensitive to metallicity

[SII] (6717, 6731) Ratio sensitive to electron density

1991ApJ...367..126C

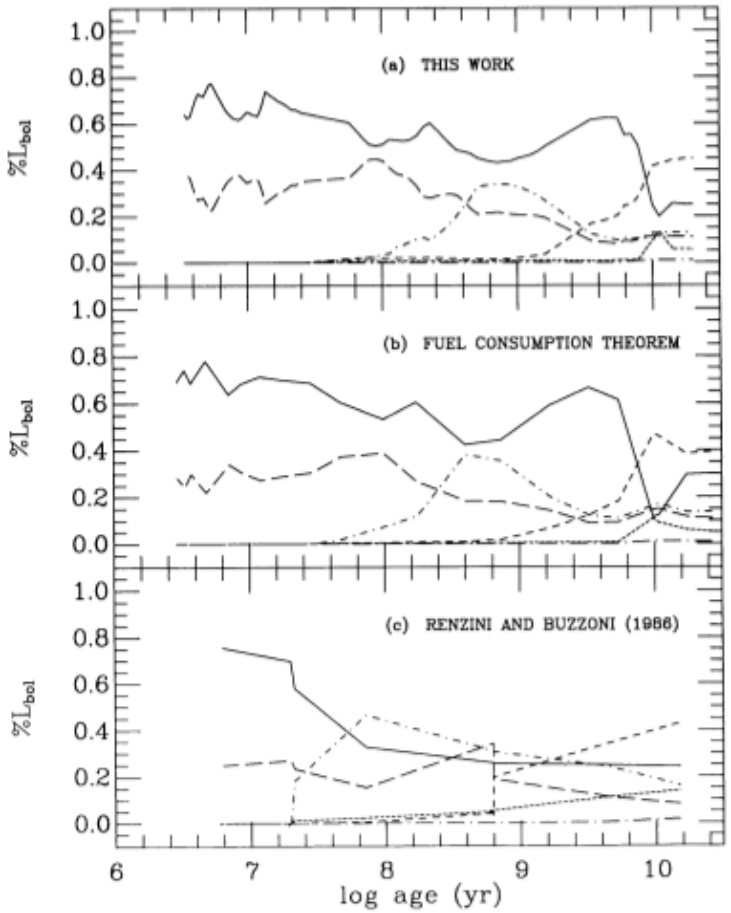

FIG. 3.—Fractional contribution of the various stellar evolutionary stages to the integrated bolometric luminosity of a burst population as a function of time (IMF from Salpeter 1955). The three panels correspond to (*a*) the isochrone synthesis model; (*b*) the fuel consumption theorem applied to the same library of tracks as in (*a*); (*c*) the results obtained by Renzini and Buzzoni (1986) by applying the fuel consumption theorem to their own library of tracks. In all panels the different curves correspond to the following stellar evolutionary stages: main sequence (*solid line*), SGB (*short-dashed line*), RGB (*dashed line*), CHeB (*long-dashed line*), AGB (*dot and short-dashed line*) and PAGB (*dot and long-dashed line*).

Solid: main sequence
Short-dash: sub-giants
Dashed: red giants
Long-dash: core He burning
Dotted: post AGB

Charlot & Bruzual 1991, ApJ

Charlot & Bruzual 1991, ApJ

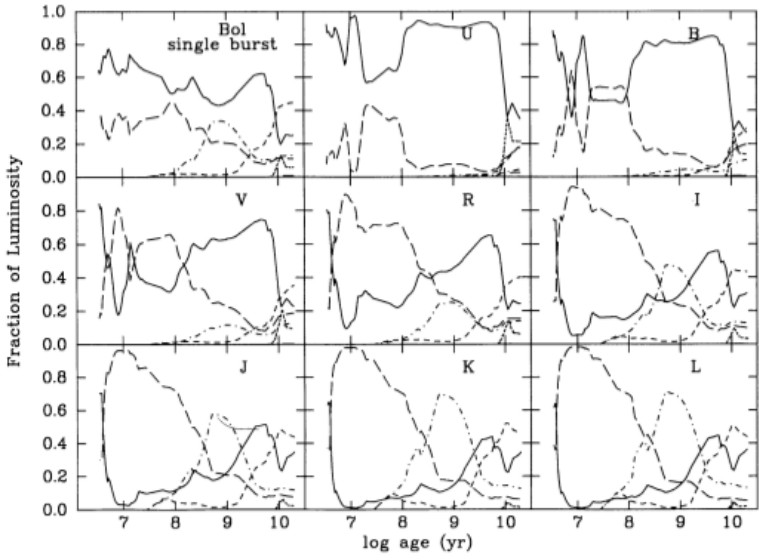

FIG. 8

FIG. 8.—Fractional contribution of the various stellar evolutionary stages to the integrated bolometric and *UBVRIJKL* luminosities of a burst population as a function of its age (IMF from Salpeter 1955). The line codes are the same as in Fig. 3.

Solid: main sequence
Short-dash: sub-giants
Dashed: red giants
Long-dash: core He burning
Dotted: post AGB

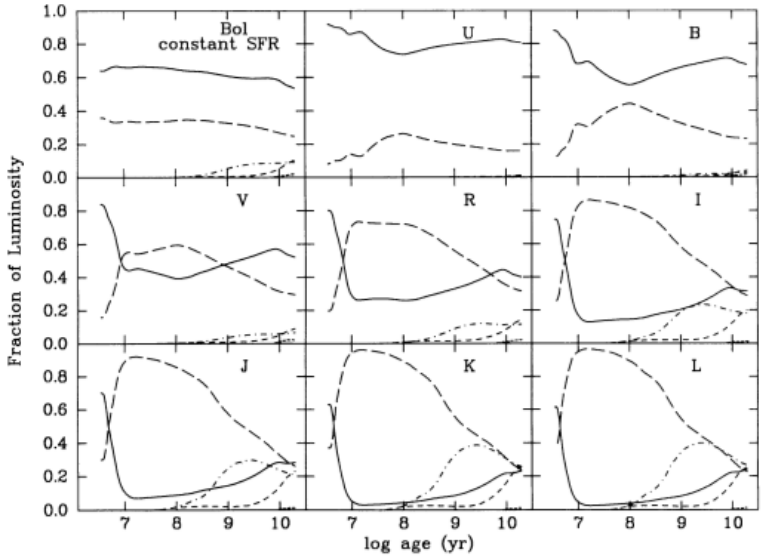

FIG. 9

FIG. 9.—Same as Fig. 8 but for a constant SFR

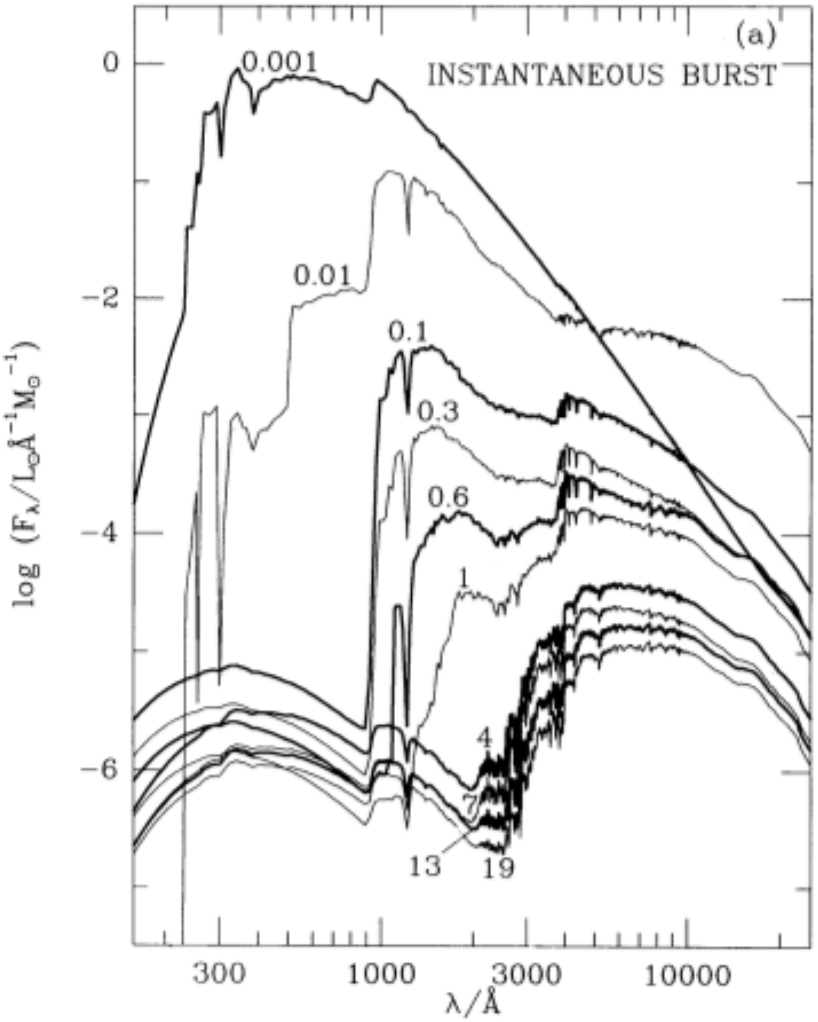

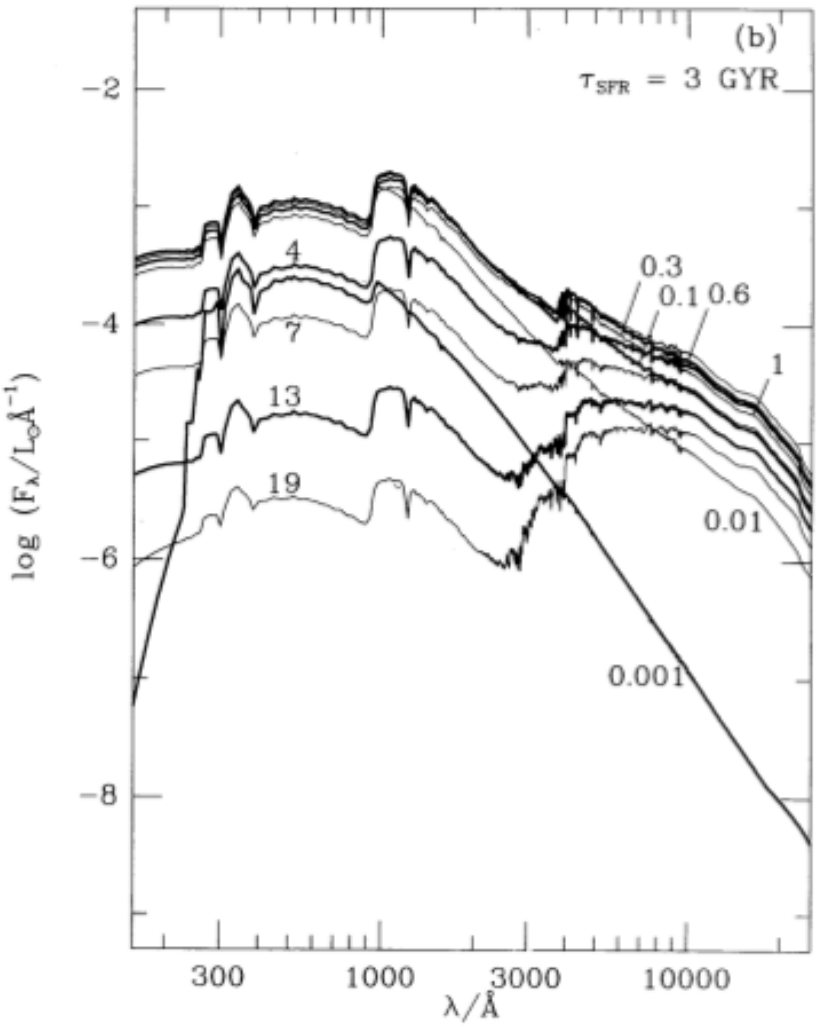

Bruzual & Charlot 1993,
ApJ, 405, 538

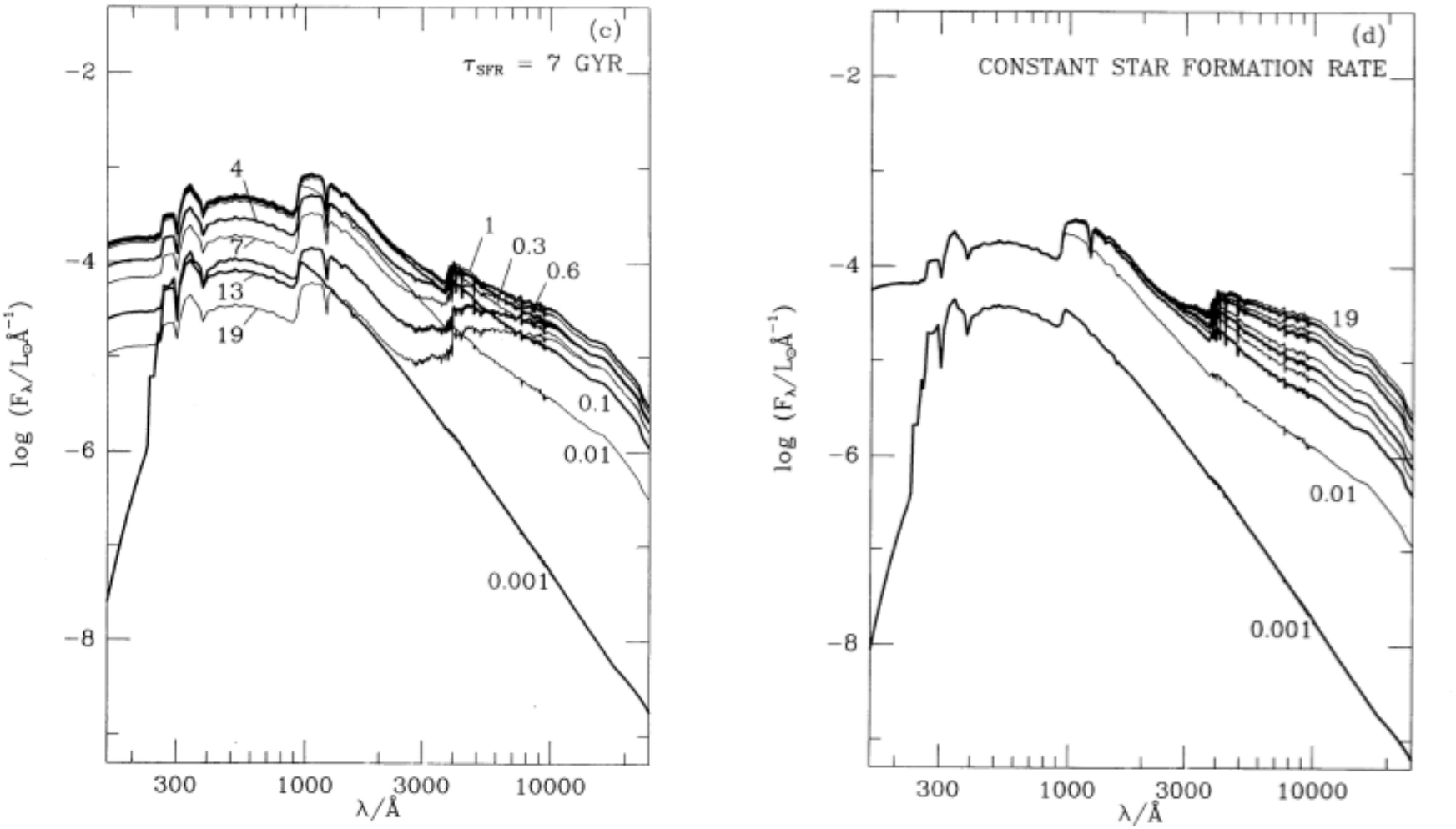

FIG. 4.—Spectral evolution of stellar populations with different star formation rates as predicted by the isochrone synthesis model: (*a*) instantaneous starburst; (*b*) eq. (2) with $\tau = 3$ Gyr; (*c*) eq. (2) with $\tau = 7$ Gyr; and (*d*) constant star formation. In each case, the age (in Gyr) is indicated next to the spectra. Thick lines and thin lines have been used alternatively for clarity. All models have the Salpeter IMF.

Bruzual & Charlot 1993, ApJ, 405, 538

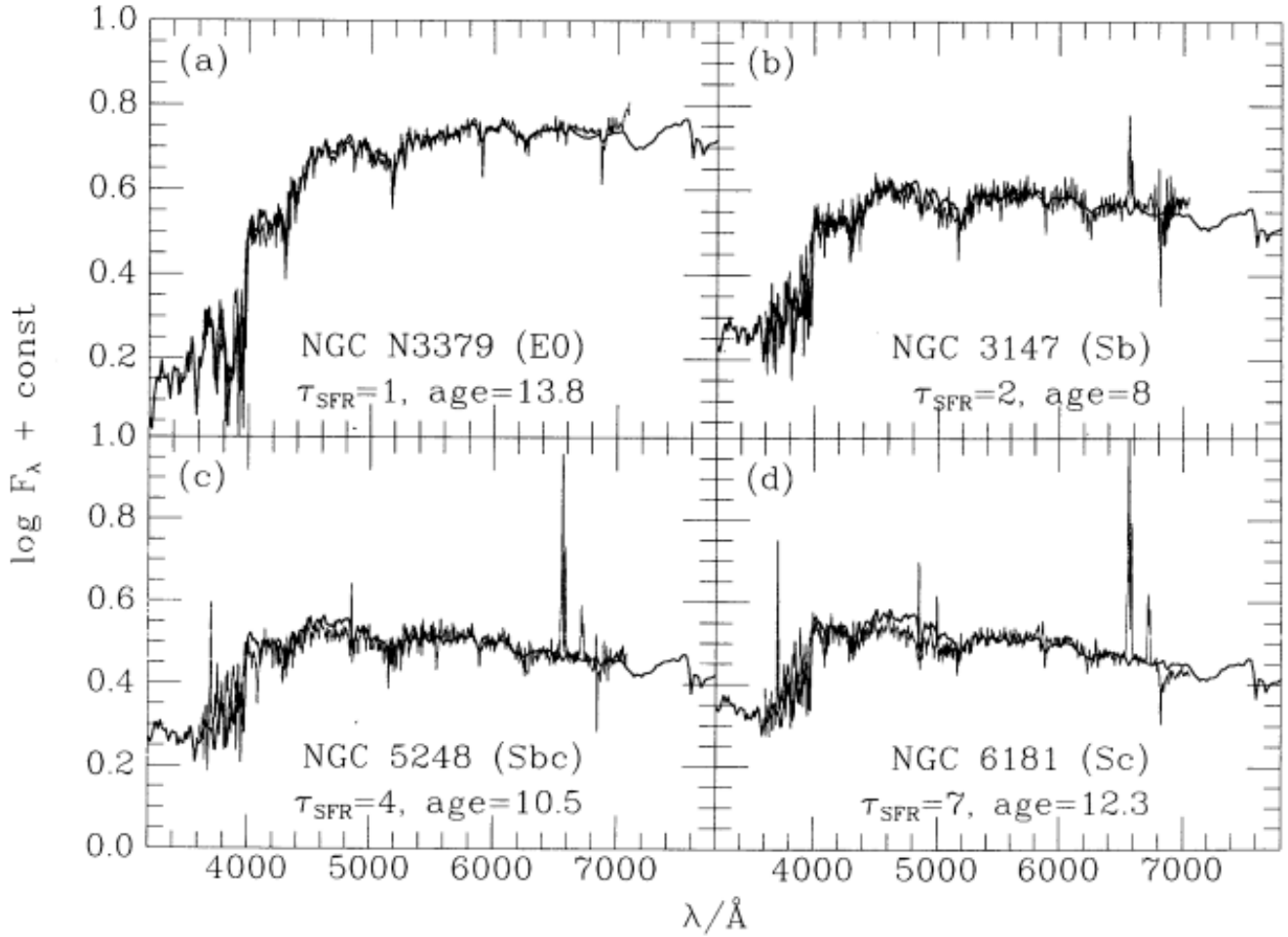

—Comparison of models with different time scales of star formation (*thick lines*) with the typical spectra of galaxies of various morphological
n Kennicutt 1992). (*a*) NGC 3379 (E0); (*b*) NGC 3147 (Sb); (*c*) NGC 5248 (Sbc); (*d*) NGC 6181 (Sc). The time scale of star formation (eq. [2]) and
are indicated (in Gyr) in each panel (see text for discussion). All models have a Salpeter IMF.

Bruzual & Charlot 1993, ApJ, 405, 538

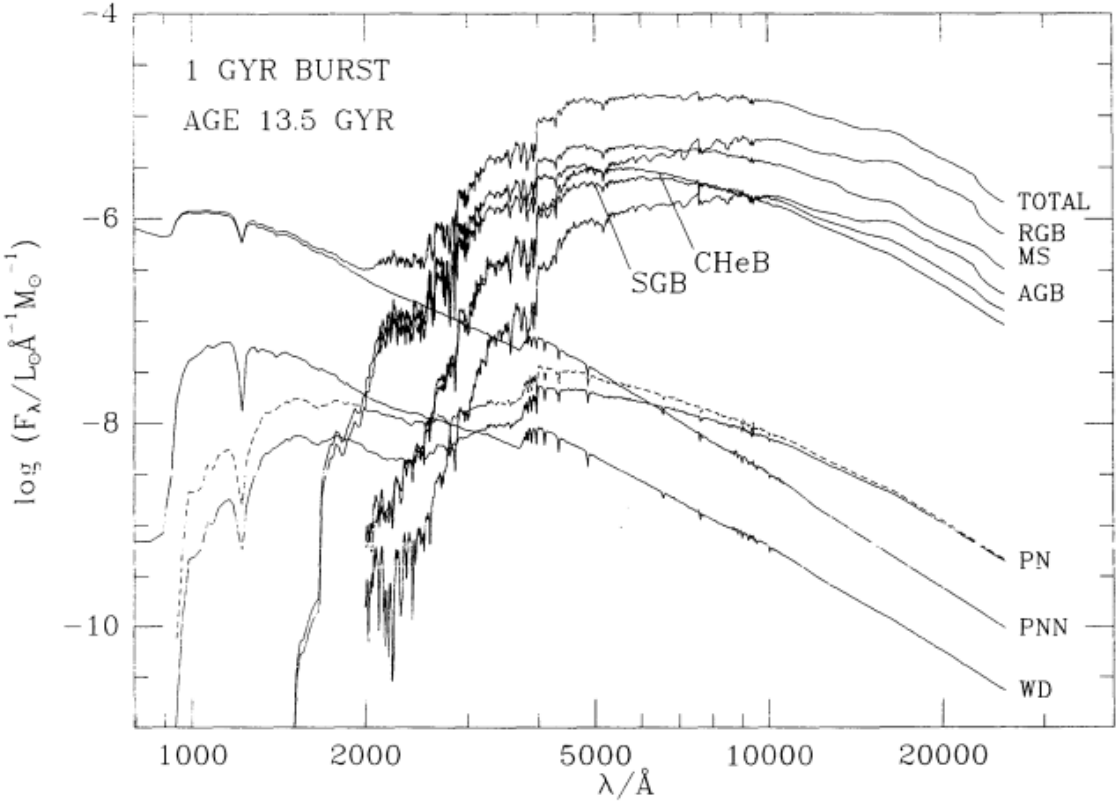

FIG. 9.—Contribution of stars in different groups to the total spectral energy distribution of a 1 Gyr burst population with the Salpeter IMF at age 13.5 Gyr. The acronyms are defined in § 3.5. The dashed line next to the PN contribution corresponds to the case where extinction of the core radiation by the surrounding nebula is ignored. The vertical scale corresponds to a total mass in stars of 1 $M_{\odot}$.

Bruzual & Charlot 1993, ApJ, 405, 538

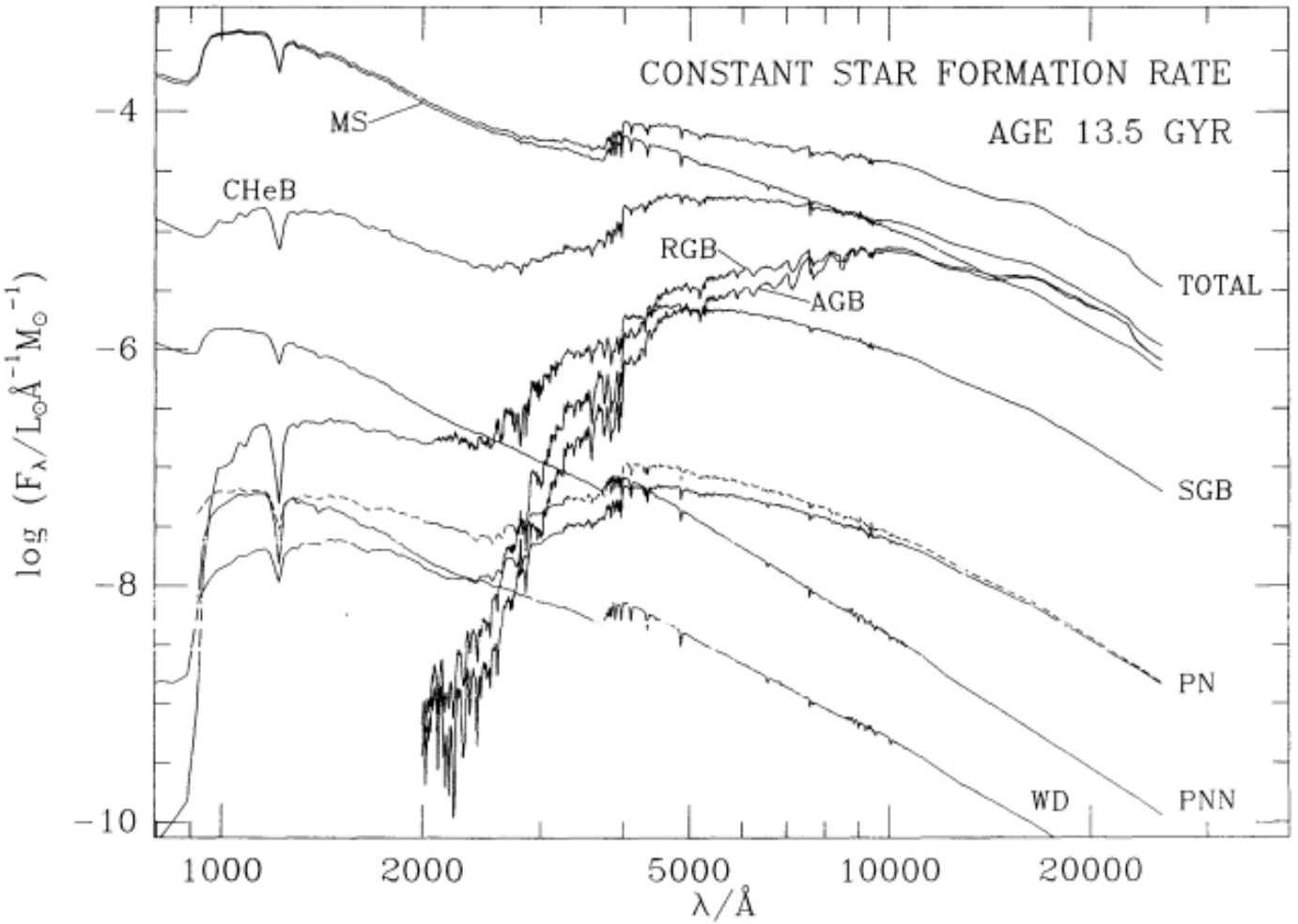

FIG. 10.—Same as Fig. 9 for a stellar population with constant star formation rate at age 13.5 Gyr

Bruzual & Charlot 1993, ApJ, 405, 538

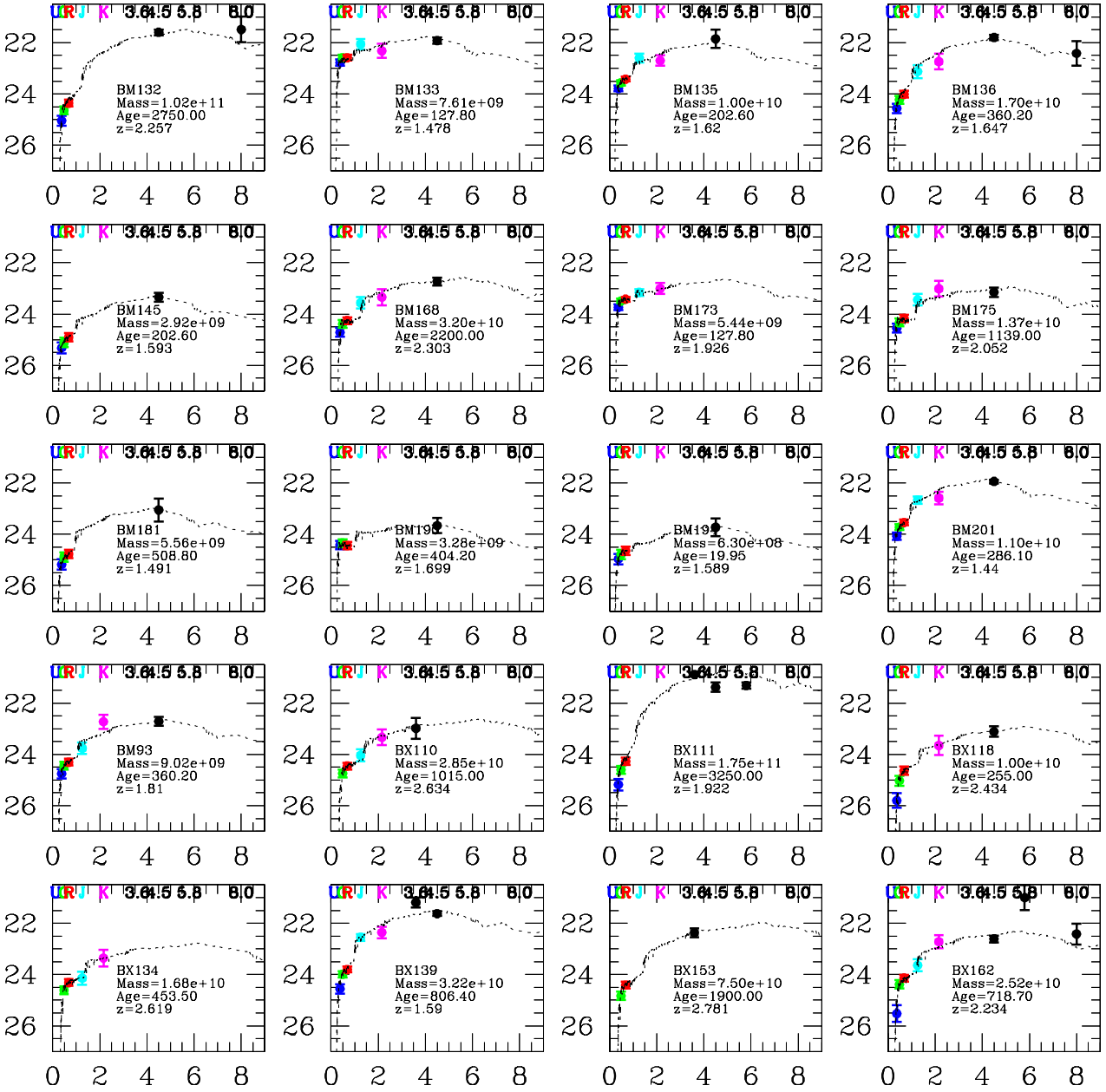
U R J K 3.6 4.5 5.8 8.0
BM132
Mass=1.02e+11
Age=2750.00
z=2.257
BM133
Mass=7.61e+09
Age=127.80
z=1.478
BM135
Mass=1.00e+10
Age=202.60
z=1.62
BM136
Mass=1.70e+10
Age=360.20
z=1.647
BM145
Mass=2.92e+09
Age=202.60
z=1.593
BM168
Mass=3.20e+10
Age=2200.00
z=2.303
BM173
Mass=5.44e+09
Age=127.80
z=1.926
BM175
Mass=1.37e+10
Age=1139.00
z=2.052
BM181
Mass=5.56e+09
Age=508.80
z=1.491
BM198
Mass=3.28e+09
Age=404.20
z=1.699
BM199
Mass=6.30e+08
Age=19.95
z=1.589
BM201
Mass=1.10e+10
Age=286.10
z=1.44
BM93
Mass=9.02e+09
Age=360.20
z=1.81
BX110
Mass=2.85e+10
Age=1015.00
z=2.634
BX111
Mass=1.75e+11
Age=3250.00
z=1.922
BX118
Mass=1.00e+10
Age=255.00
z=2.434
BX134
Mass=1.68e+10
Age=453.50
z=2.619
BX139
Mass=3.22e+10
Age=806.40
z=1.59
BX153
Mass=7.50e+10
Age=1900.00
z=2.781
BX162
Mass=2.52e+10
Age=718.70
z=2.234
22
24
26
0 2 4 6 8

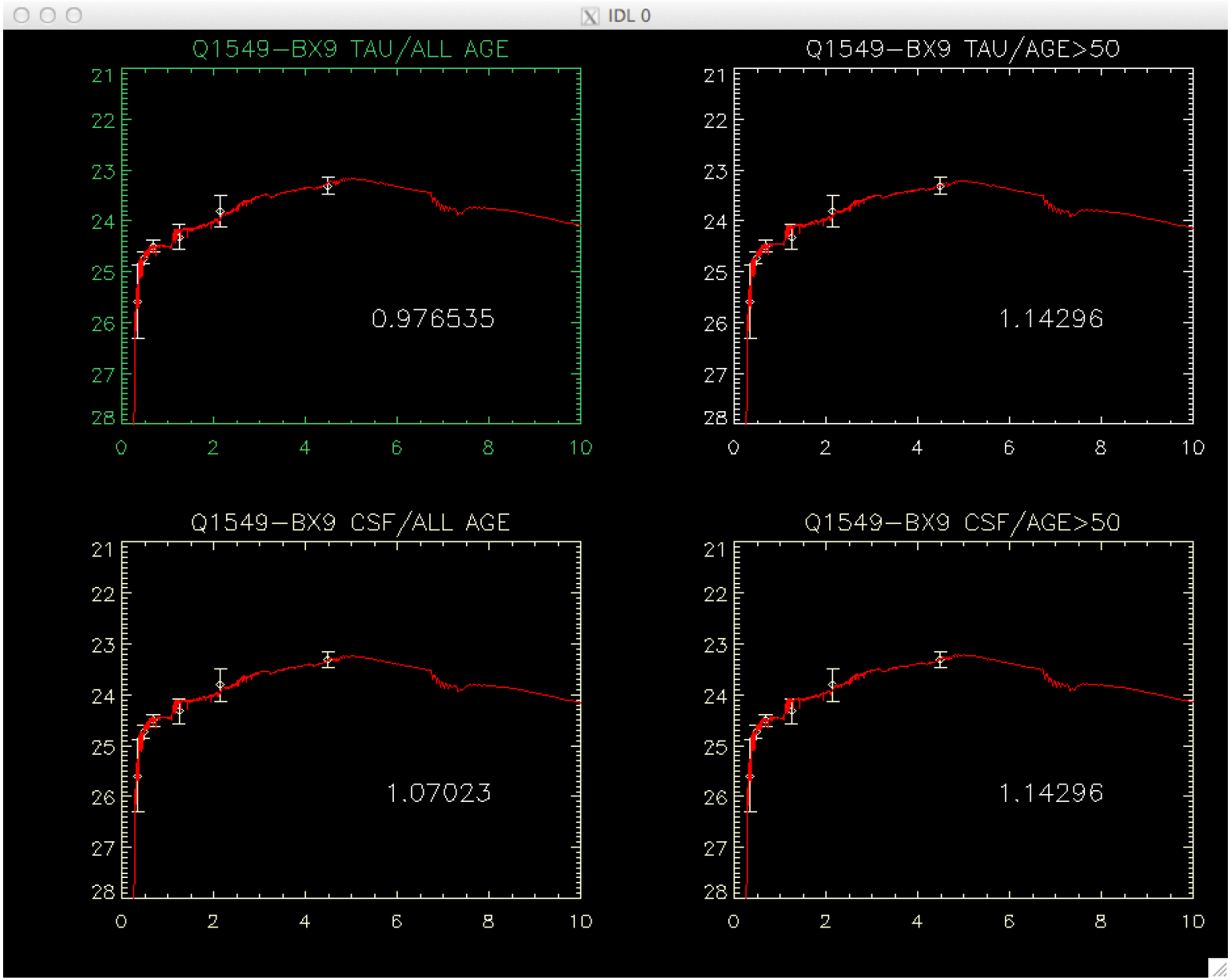

Z=1.949 M*=2e9 $M_\odot$ SFR=39 $M_\odot$/yr E(B-V)=0.2 age=50Myr

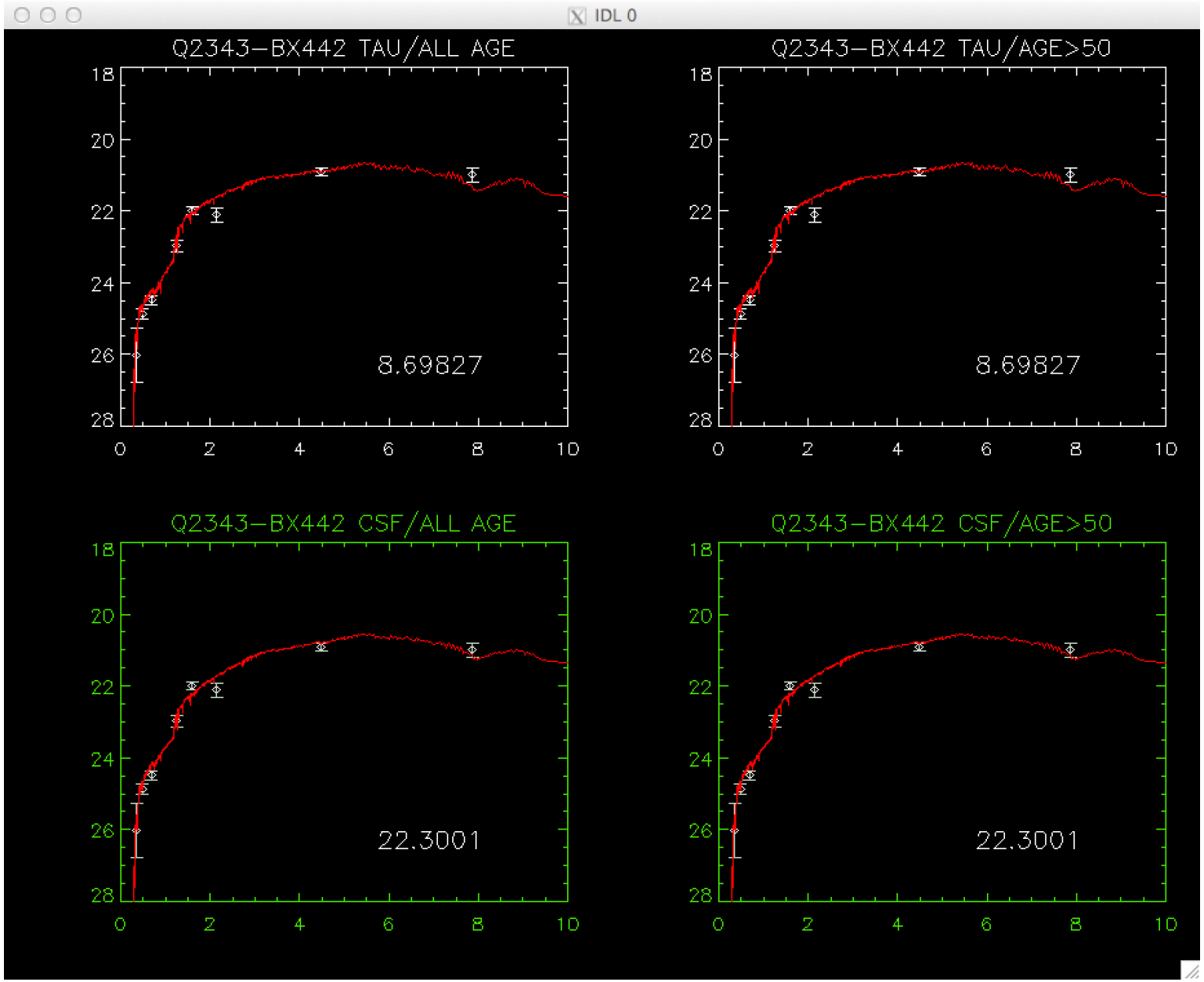

z=2.177 M*=2.3e11 $M_\odot$ SFR=90 $M_\odot$/yr E(B-V)=0.28 age=2600 Myr